CrossMark

J. Fluid Mech. (2018), *vol.* 846, *pp.* 536–562. © Cambridge University Press 2018
doi:10.1017/jfm.2018.263

Singularity formation on perturbed planar shock waves

W. Mostert[1,†], D. I. Pullin[1], R. Samtaney[2] and V. Wheatley[3]

[1]Graduate Aerospace Laboratories, California Institute of Technology, CA 91125, USA

[2]Mechanical Engineering, Physical Sciences and Engineering Division, King Abdullah University of Science and Technology, Thuwal, Saudi Arabia, 23955-6900

[3]School of Mechanical and Mining Engineering, University of Queensland, QLD 4072, Australia

(Received 28 June 2017; revised 7 March 2018; accepted 16 March 2018;
first published online 8 May 2018)

We present an analysis that predicts the time to development of a singularity in the shape profile of a spatially periodic perturbed, planar shock wave for ideal gas dynamics. Beginning with a formulation in complex coordinates of Whitham's approximate model geometrical shock dynamics (GSD), we apply a spectral treatment to derive the asymptotic form for the leading-order behaviour of the shock Fourier coefficients for large mode numbers and time. This is shown to determine a critical time at which the coefficients begin to decay, with respect to mode number, at an algebraic rate with an exponent of $-5/2$, indicating loss of analyticity and the formation of a singularity in the shock geometry. The critical time is found to be inversely proportional to a representative measure of perturbation amplitude ϵ with an explicit analytic form for the constant of proportionality in terms of gas and shock parameters. To leading order, the time to singularity formation is dependent only on the first Fourier mode. Comparison with results of numerical solutions to the full GSD equations shows that the predicted critical time somewhat underestimates the time for shock–shock (triple-point) formation, where the latter is obtained by post-processing the numerical GSD results using an edge-detection algorithm. Aspects of the analysis suggest that the appearance of loss of analyticity in the shock surface may be a precursor to the first appearance of shock–shocks, which may account for part of the discrepancy. The frequency of oscillation of the shock perturbation is accurately predicted. In addition, the analysis is extended to the evolution of a perturbed planar, fast magnetohydrodynamic shock for the case when the external magnetic field is aligned parallel to the unperturbed shock. It is found that, for a strong shock, the presence of the magnetic field produces only a higher-order correction to the GSD equations with the result that the time to loss of analyticity is the same as for the gas-dynamic flow. Limitations and improvements for the analysis are discussed, as are comparisons with the analogous appearance of singularity formation in vortex-sheet evolution in an incompressible inviscid fluid.

Key words: compressible flows, shock waves

† Present address: Mechanical & Aerospace Engineering, Princeton University, NJ 08544, USA. Email address for correspondence: wouter.mostert@uqconnect.edu.au

https://doi.org/10.1017/jfm.2018.263 Published online by Cambridge University Press

1. Introduction

It is well known that planar gas-dynamic shock waves are stable in the sense that the amplitude of an initially small perturbation on the surface of such shocks decays over time t (Whitham 1957). Indeed, the problem has been studied in some depth in both theoretical and experimental contexts by Chisnell (1957), Freeman (1957) and others. It is also known that shocks can develop singularities in their geometry, identified as triple points or Mach stems, as appropriate. In reacting flows the formation of diamond-shaped cellular patterns in the flow downstream of detonation waves is of ongoing research interest; see for example Majda & Rosales (1983) and Faria, Kasimov & Rosales (2015). These involve in some measure the development of singularities on the shock surface.

Geometrical shock dynamics (GSD) (Whitham 1957) is a model of shock motion. It is based on the kinematic assumption that differential elements of the shock propagate along rays normal to the shock surface, at a Mach number computed from the local shock curvature through an area–Mach-number relation. This relation is derived from the quasi-one-dimensional Euler equations for the case of a shock propagating along a tube of non-uniform area. GSD is phenomenological in the sense that, while it contains the characteristic equation and the shock-jump conditions, it is not formally derived from the Euler equations. In the language of GSD, shock-profile singularities are known as 'shock–shocks', that is, discontinuities in the shock-profile gradient (Whitham 1957). In addition to the examples in reacting flow, shock–shocks have appeared both in numerical contexts, particularly in studies of GSD by Henshaw, Smyth & Schwendeman (1986) and Schwendeman (1993) in planar and converging geometries, and in experiment, where Watanabe & Takayama (1991) observed the mild geometric instability of converging cylindrical shocks where these shock–shocks play a prominent role. The appearance of shock–shocks thus appears to be incidental to the stability of the shock in the sense described above.

Several studies demonstrate numerically the transition of an initially smooth shock profile to a faceted shock (that is, a shock with shock–shocks), for example Schwendeman (1993), Mostert *et al.* (2017) and the studies cited above. Whitham (1957) suggests an analogy for shock–shock formation from an initially smooth, almost planar shock based on the Burgers equation. This suggests a formation time proportional to $1/\epsilon$, where ϵ is a representative perturbation amplitude, in agreement with numerical solutions of the GSD equation (Mostert *et al.* 2017) but does not provide a mechanistic scenario for the origin of shock–shocks in terms of shock evolution physics nor a quantitative estimate of the dependence of the formation time on gas properties and shock-wave parameters. Motivated by the study of detonation waves, Clavin (2013) investigates formation of Mach stems in shocks following interaction with weak vortices in inert gases, under linear and weakly nonlinear analytical formulations, and provides scaling results for the time to Mach stem formation depending on the strength of the perturbation in the distinguished limit $M \to \infty$, $M^2(\gamma - 1) \to 1$ (where M is shock Mach number and γ is specific heat ratio). These results show good agreement for the trajectories of late-time triple points in the distinguished limit from the Navier–Stokes simulations of Denet *et al.* (2015) and Lodato, Vervisch & Clavin (2016, 2017), but do not provide analytical estimates of the functional dependence of the time to spontaneous triple point formation on flow parameters.

In this study we employ a spectral treatment of the approximate GSD equations which seeks to predict the formation of a singularity in some derivative of the perturbation on a spatially periodic, initially smooth evolving shock surface in two

https://doi.org/10.1017/jfm.2018.263 Published online by Cambridge University Press

spatial dimensions. The analysis utilizes in part a method for analysis of the decay of the Fourier coefficients as a function of both time and mode number developed by Moore (1979) in the context of vortex-sheet evolution in an ideal incompressible fluid. We consider a shock wave propagating in an ideal gas with given constant ratio of specific heats and with given Mach number of the unperturbed shock, subject to a rather general class of spatially periodic initial conditions. A critical time is found at which the rate of decay behaviour with respect to the mode number of Fourier coefficients of the shock geometry and perturbed Mach-number distribution changes from exponential to algebraic. This is the signature of the appearance of a spontaneous loss of analyticity of the shock profile. An important issue to be discussed is whether the singularity formation time can be identified closely with the formation of a shock–shock.

In § 2 we derive, using Whitham's geometrical shock dynamics (GSD), a single equation in complex coordinates that describes the evolution of a gas-dynamic shock wave with general shock shape and Mach-number profile. The limits of this equation for both small and large Mach number respectively are then explored. For the case of strong shocks, a Fourier method is used in § 3 to obtain nonlinear equations that describe the time-wise evolution of the Fourier components. Admissible initial conditions are discussed in § 4 while in § 5 simplifying assumptions are introduced that enable, using a generating-function method (Moore 1979), reduction to a recursive series of paired linear inhomogeneous ordinary differential equations (ODEs) for which a self-consistent form of the coefficients for large mode number can be found to leading order. This is then shown to give a critical time at which exponential decay with respect to mode number is lost, corresponding to loss of analyticity in the description of both the geometrical shock shape and its Mach-number distribution. Section 6 extends the result to small and general Mach numbers while in § 7 a restricted magnetohydrodynamic (MHD) case is considered. In § 8 the analytical prediction is compared with numerical results using the GSD code of Mostert *et al.* (2017), using an edge-detection diagnostic to find the time of shock–shocks. Discussion and interpretation of these results are given in § 9. We conclude in § 10 with some comments on the potential adaptation of the analysis to weak shocks and cylindrical or spherical converging shocks.

2. Development of evolution equation

The evolution in time of a planar two-dimensional shock wave, whose surface is described in real space by the vector $\boldsymbol{x} = (x, y)^{\mathrm{T}}$ and parametrized periodically along its surface with $\beta \in [0, 2\pi)$, can be approximated by the following equation of geometrical shock dynamics (GSD) (Whitham 1957):

$$\frac{\partial \boldsymbol{x}}{\partial t} = a_0 M(\beta, t)\boldsymbol{n}(\beta, t), \tag{2.1}$$

where M is the Mach number of the shock, a_0 is the sound speed ahead of the shock and $\boldsymbol{n} = (\cos(\theta(\beta, t)), \sin(\theta(\beta, t)))$ is the unit vector normal to the shock. These equations are taken to be non-dimensionalized according to a reference velocity $\sqrt{p_0/\rho_0}$, where p_0 and ρ_0 are reference pressure and density respectively, and length scale L, where $2\pi L$ is the largest initial perturbation wavelength. We assume the gas ahead of the shock is in a spatially and temporarily uniform state. It will be convenient to treat this as a single-variable system by writing the shock position in complex coordinates,

$$Z(\beta, t) = \beta + \mathrm{i}a_0 M_0 t + z(\beta, t), \tag{2.2}$$

$$z(\beta, t) = x_1(\beta, t) + \mathrm{i}y_1(\beta, t), \tag{2.3}$$

https://doi.org/10.1017/jfm.2018.263 Published online by Cambridge University Press

so that (2.1) is now

$$\frac{\partial Z}{\partial t} = \mathrm{i}a_0 M(\beta, t) s(\beta, t), \tag{2.4}$$

where $s(\beta, t) = -\mathrm{i}n$ is the unit tangent vector, and n the unit normal in complex form. With $Z(\beta, t)$ defined thus, in this form the unperturbed shock extends in the real direction and travels in the imaginary direction with constant Mach number M_0, and $z(\beta, t)$ is a perturbation on its surface, which in turn perturbs its motion. We seek to investigate the possible existence of a time at which $z(\beta, t)$ loses analyticity in β corresponding to the formation of a singularity in some derivative of the surface. While (2.4) is an exact kinematic description of a surface that moves normal to itself as stated, in order to construct a dynamical equation for shock propagation, a closure relation for $M(\beta, t)$ must be provided, and this is in general obtained from an approximate area–Mach number relation. In gas dynamics this closure has the form

$$\frac{f(M)}{f(M_0)} = \frac{A}{A_0}, \tag{2.5}$$

where

$$f(M) = \exp\left(-\int \frac{M\lambda(M)}{M^2 - 1}\,\mathrm{d}M\right) \tag{2.6}$$

and A is a variable proportional to the cross-sectional area between two adjacent rays normal to the shock surface (Whitham 1957), or the ray-tube area. $\lambda(M)$ is a known, explicit function of M. Equation (2.5) is bijective from $M \in (1, \infty)$ onto $A \in (0, \infty)$ so that there is an inverse relation

$$M = q(A) = f^{-1}(A), \tag{2.7}$$

which closes (2.1) provided we can find a suitable function $A = A(\beta)$. The parametrization along the shock with β corresponds to a parametrization of the rays perpendicular to the shock. In this sense, β may be thought of as a Lagrangian label for a given ray. Then, since A is proportional to the ray-tube area, it can be thought of as the local 'stretchedness' of the shock (hence the treatment in Henshaw *et al.* (1986)), which is given as the arclength derivative of Z with respect to β,

$$A = A_0 \sqrt{\frac{\partial Z}{\partial \beta}\frac{\partial Z^*}{\partial \beta}}, \tag{2.8}$$

where A_0 is a 'reference area' acting as the proportionality constant. Using the definition of the unit tangent s from curve theory, we arrive at

$$\frac{\partial Z}{\partial t} = \mathrm{i}a_0 M_0 \frac{q(A)}{q(A_0)} \frac{\partial Z}{\partial \beta}\left(\frac{\partial Z}{\partial \beta}\frac{\partial Z^*}{\partial \beta}\right)^{-1/2}. \tag{2.9}$$

Equation (2.9) is essentially a nonlinear wave equation, but it is not suitable for our present purpose because $q(A)$ can in general only be calculated numerically. We can simplify the problem for the cases where the Mach number is small ($M - 1 \ll 1$) or large ($M \gg 1$). Later we will discuss a general solution method for (2.9).

https://doi.org/10.1017/jfm.2018.263 Published online by Cambridge University Press

2.1. *Large Mach-number limit*

In the strong-shock limit, $M \gg 1$, shock dynamics provides the asymptotic relation

$$q(A) = A^{-1/p}(\beta, t), \tag{2.10}$$

where

$$p \equiv p(\gamma) = 1 + \frac{2}{\gamma} + \sqrt{\frac{2\gamma}{\gamma - 1}}, \tag{2.11}$$

γ being the (constant) ratio of specific heats, so that

$$\frac{\partial Z}{\partial \tau} = \mathrm{i}\left(\frac{\partial Z}{\partial \beta}\frac{\partial Z^*}{\partial \beta}\right)^{-(p+1/2p)}\frac{\partial Z}{\partial \beta}, \tag{2.12}$$

where the variable transformation $\tau = a_0 M_0 t$ scales the constants M_0, a_0 out of the system. Strictly, τ is space-like but we will refer to it as a re-scaled time for convenience of interpretation. We study this formulation because it is relatively simpler than (2.9) and allows for a straightforward Fourier representation.

Equation (2.12) describes the evolution in time of the entire shock. It can be written in terms of the perturbation $z(\beta, \tau)$ on the motion of the flat shock, $Z_0(\beta, \tau) = \beta + \mathrm{i}\tau$, by using (2.2) and (2.3). Using the shorthand $D = \partial/\partial\beta$ we obtain

$$\frac{\partial z}{\partial \tau} + \mathrm{i} = \mathrm{i}[(1 + Dz)(1 + Dz^*)]^{-(p+1/2p)}(1 + Dz), \tag{2.13}$$

noting that since β is real, $Dz^* = D(z^*) = (Dz)^*$. Equation (2.13) will be the main focus of this study.

To leading order (2.13) is also valid for strong, fast MHD shocks which are parallel to an applied (uniform) magnetic field ahead of the shock in the mean. This corresponds to MHD shocks where the magnetosonic Mach number $M_f = Ma_0/c_{f0} \gg 1$, where c_{f0} is the magnetosonic speed for a parallel field ahead of the shock. This is because $M_f \gg 1$ implies $M \gg 1$ and it is shown in appendix A that in this limit the gas-dynamic result (2.10) is recovered with a small correction. This case is presented briefly in § 7. The weak-shock MHD case ($M_f - 1 \ll 1$) is not considered here.

2.2. *Small Mach-number limit*

When the gas-dynamic shock is weak, that is when $M - 1 \ll 1$, then the asymptotic relation between M and A is

$$\frac{(M-1)^2}{(M_0-1)^2} \sim \frac{A_0}{A}. \tag{2.14}$$

By substitution directly into (2.4), we have

$$\frac{\partial Z}{\partial t} = \mathrm{i}a_0\left[(M_0 - 1)\left(\frac{\partial Z}{\partial \beta}\frac{\partial Z^*}{\partial \beta}\right)^{-1/4} + 1\right]\frac{\partial Z}{\partial \beta}\left(\frac{\partial Z}{\partial \beta}\frac{\partial Z^*}{\partial \beta}\right)^{-1/2}. \tag{2.15}$$

This equation may be treated by the same substitution of $z = Z - (\beta + \mathrm{i}a_0 M_0 t)$ as for (2.13).

https://doi.org/10.1017/jfm.2018.263 Published online by Cambridge University Press

3. Truncated Fourier representation for strong shocks

We proceed with the spectral treatment of (2.13). In the sequel this treatment will be adapted to (2.15) and (2.9). Now $(1+Dz)(1+Dz^*)=1+Dz+Dz^*+DzDz^*$. Assuming that the perturbation z and its first derivative Dz both exist, and are small, then since $|Dz+Dz^*+DzDz^*|\ll 1$, the exponentiated quantity in (2.13) may be expanded in a convergent binomial series, and

$$\frac{\partial z}{\partial \tau}+\mathrm{i}=\mathrm{i}[1+Dz+P(\beta)+DzP(\beta)], \tag{3.1}$$

where

$$P(\beta)=\sum_{k=1}^{\infty} b_k(Dz+Dz^*+DzDz^*)^k, \tag{3.2}$$

$$b_k=\binom{-(p+1)/(2p)}{k}. \tag{3.3}$$

With $z(\beta,\tau)$ analytic, it has a Fourier representation in β

$$z(\beta,\tau)=\sum_{m=-\infty}^{\infty}\hat{z}_m(\tau)\mathrm{e}^{\mathrm{i}m\beta} \tag{3.4}$$

along with derivatives

$$Dz=\sum_{m=-\infty}^{\infty}\mathrm{i}m\hat{z}_m\mathrm{e}^{\mathrm{i}m\beta},\quad Dz^*=\sum_{m=-\infty}^{\infty}\mathrm{i}m\hat{z}^*_{-m}\mathrm{e}^{\mathrm{i}m\beta}, \tag{3.5a,b}$$

$$DzDz^*=\sum_{m=-\infty}^{\infty}\mathrm{e}^{\mathrm{i}m\beta}\sum_{r_1+r_2=m}\mathrm{i}^2r_1r_2\hat{z}_{r_1}\hat{z}^*_{-r_2}. \tag{3.6}$$

The quantity (3.6) is an infinite discrete convolution. Both sums are infinite. Then $P(\beta)$ expanded to $k=2$ is

$$\begin{aligned}P(\beta)\equiv\sum_{m=-\infty}^{\infty}\mathrm{e}^{\mathrm{i}m\beta}P_m=\sum_{m=-\infty}^{\infty}\mathrm{e}^{\mathrm{i}m\beta}\Bigg[&b_1\left(\mathrm{i}m(\hat{z}_m+\hat{z}^*_{-m})+\sum_{r_1+r_2=m}\mathrm{i}^2r_1r_2\hat{z}_{r_1}\hat{z}^*_{-r_2}\right)\\&+b_2\Bigg(\sum_{r_1+r_2=m}\mathrm{i}^2r_1r_2(\hat{z}_{r_1}+\hat{z}^*_{-r_1})(\hat{z}_{r_2}+\hat{z}^*_{-r_2})\\&+2\sum_{r_1+r_2+r_3=m}\mathrm{i}^3r_1r_2r_3(\hat{z}_{r_1}+\hat{z}^*_{-r_1})\hat{z}_{r_2}\hat{z}^*_{-r_3}\\&+\sum_{r_1+r_2+r_3+r_4=m}\mathrm{i}^4r_1r_2r_3r_4\hat{z}_{r_1}\hat{z}^*_{-r_2}\hat{z}_{r_3}\hat{z}^*_{-r_4}\Bigg)+\cdots\Bigg].\end{aligned} \tag{3.7}$$

The term in the second line of (3.7) is a second-order convolution, like (3.6). The term in the third line is a third-order convolution, and in the fourth line, a fourth-order convolution. Multiplication of $P(\beta)$ by Dz, as in (3.1), will increase the order of each term by one. We will show later that in treating (3.1) we need only retain second-order

https://doi.org/10.1017/jfm.2018.263 Published online by Cambridge University Press

terms, which will simplify the analysis considerably. Now note that the convolutions preserve $e^{im\beta}$, and we may equate the coefficients of the $e^{im\beta}$ so that (3.1) becomes an infinite set of coupled ordinary differential equations (ODEs) and may be written purely in terms of the Fourier coefficients,

$$\frac{d\hat{z}_0}{d\tau} = i[P_0 + (DzP)_0], \quad m = 0, \tag{3.8}$$

$$\frac{d\hat{z}_m}{d\tau} = i[(Dz)_m + P_m + (DzP)_m], \quad m \neq 0. \tag{3.9}$$

The subscript m on P indicates the mth term of (3.7), and similarly for Dz and DzP. In particular, $(DzP)_m$ is the mth Fourier mode of the convolution of Dz and P. Hence for a given m, P_m and $(DzP)_m$ are infinite sums, each term in each sum involving infinite convolutions of all other coefficients $\hat{z}_{r_i}$. Equation (3.9) is intractable but can be simplified considerably by some leading-order approximations that result from the initial condition (§ 4). The ODE (3.8) expresses the motion of the unperturbed shock, but does not influence any coefficients with $m \neq 0$.

4. Choice and effect of initial condition

Consider an initial perturbation on the shock at $\tau = 0$,

$$z(\beta, 0) = \sum_{m=-\infty}^{\infty} B_m e^{im\beta}, \tag{4.1}$$

which is a general Fourier perturbation. This is the initial condition (IC). The contribution from the first mode $|m| = 1$ is

$$z_{\pm 1}(\beta, 0) = B_1 \exp[i(\beta)] + B_{-1} \exp[-i(\beta)], \tag{4.2}$$

where B_1, B_{-1} are complex. In the choice of this IC there are two degrees of freedom, since the amplitude and phase of B_{-1} can be chosen in terms of those of B_1. Without loss of generality then, set

$$B_1 = -i\frac{\epsilon}{2}, \quad B_{-1} = \sigma B_1, \quad \sigma \in \mathbb{C}, |\sigma| \leqslant 1, \tag{4.3a–c}$$

which defines $\epsilon \ll 1$ as a nominal perturbation amplitude. Then clearly,

$$\hat{z}_1(0) = -i\frac{\epsilon}{2}, \quad \hat{z}_{-1}(0) = \sigma \hat{z}_1(0). \tag{4.4a,b}$$

In this way the choice of the first mode in the IC is general except for the constraint that $\epsilon \ll 1$. The higher modes may now be specified as follows:

$$B_{\pm m} = \frac{B_{\pm 1}}{\epsilon} h(m) e^{|m| \log \epsilon}, \tag{4.5}$$

such that $h(m)$ is a complex-valued function for which $h(1) = 1$ and which may grow at up to any algebraic rate (any greater growth with m would destroy analyticity of the IC). The constraint on the exponent ensures that initially $\hat{z}_m = O(\epsilon^{|m|})$. Note that these constraints are trivially satisfied by choosing any single mode perturbation with

https://doi.org/10.1017/jfm.2018.263 Published online by Cambridge University Press

amplitude ϵ. We emphasize that the IC thus constructed is a general analytic function with only a weak constraint on its Fourier spectrum.

We now assume that for a range of times τ, all coefficients $\hat{z}_m = O(\epsilon^{|m|})$, subject to consistency with the end solution. This would result from a choice of the IC such that at early times $\hat{z}_{\pm 1}$ are the largest and $O(\epsilon)$, while all other coefficients are smaller so that any convolved term of order $\pm|m|$, for instance, on the right-hand side of (3.9) is at its largest when the $r_1 = r_2 = r_3 = \cdots = r_m = \pm 1$.

This estimate fails if there are modes $\hat{z}_m$ which very quickly grow to be greater than $O(\epsilon)$. But this cannot happen from (4.4*a*,*b*) since, again, the maximum contribution to $\hat{z}_m$ can only be through an up to mth-order convolution of the $\hat{z}_{\pm 1}$, which is by construction $O(\epsilon^{|m|})$.

This implies that each $\hat{z}_m$ has a representation

$$\hat{z}_m = \epsilon^{|m|} \sum_{j=0}^{\infty} R_{m,j} \epsilon^j, \tag{4.6}$$

of which the leading-order term is obviously $R_{m,0}\epsilon^{|m|}$. Substituting (4.6) into (3.9) divides the system into subsystems for the $R_{m,j}$, for which the jth subsystem is not dependent on the subsystems $j+1$. In principle, solutions to the jth subsystem may be obtained if the solutions to all subsystems for the $R_{m,i}$, $i < j$ are known. Here we consider only the leading-order subsystem, writing $\tilde{R}_m = R_{m,0}$ for convenience,

$$\frac{\mathrm{d}\tilde{R}_m}{\mathrm{d}\tau} = \mathrm{i}\left[\widetilde{(DR)}_m + \widetilde{P}_m + \widetilde{(PDR)}_m\right], \quad m \neq 0, \tag{4.7}$$

where

$$\tilde{P}_m = b_1 \left[\mathrm{i}m(\tilde{R}_m + \tilde{R}^*_m) + \sum_{\substack{r_1+r_2=m,\\ r_1,r_2 \geqslant 1}} \mathrm{i}^2 r_1 r_2 \tilde{R}_{r_1} \tilde{R}^*_{-r_2} \right] + \cdots \tag{4.8}$$

and similarly for the other terms. Note that the convolutions are now constrained to partitions over $r_i \geqslant 1$ so that they are no longer infinite. To illustrate, for a second-order convolution in $m = 2$, the leading-order contribution can only come from $r_1 = r_2 = |1|$ (an $O(\epsilon^2)$ contribution), since, say, $r_1 = 3$, $r_2 = -1$ is an $O(\epsilon^4)$ contribution and hence belongs to a higher-order subsystem of (3.9) and not to (4.7).

5. Asymptotic behaviour of the Fourier coefficients

5.1. *Development of solution form*

The equations (4.7) form a system of linear, inhomogeneous ODEs, except for the case $|m| = 1$ which is homogeneous. For a given $m > 0$, we have the positive and negative modes given by

$$\frac{\mathrm{d}R_m}{\mathrm{d}\tau} = -mR_m - mb_1(R_m + R^*_{-m}) + \mathrm{i}f_m, \tag{5.1}$$

$$\frac{\mathrm{d}R_{-m}}{\mathrm{d}\tau} = mR_{-m} + mb_1(R_{-m} + R^*_m) + \mathrm{i}f_{-m}, \tag{5.2}$$

dropping the tildes for convenience. $f_{\pm m}$ is a forcing term depending only on the lower mode solutions R_j, $j < m$. Solving sequentially $|m| = 1, 2, 3, \ldots$ the forcing term is

https://doi.org/10.1017/jfm.2018.263 Published online by Cambridge University Press

therefore always known in terms of the lower mode solutions, and hence in principle all the solutions may be produced recursively. However, we desire the behaviour of the R_m for $m \gg |1|$ which is unfeasible to produce in this manner. But if the general form of $R_m(\tau)$ can be deduced, then it is possible to determine the behaviour of these coefficients asymptotically without the need for recursive solutions. We do this as follows. Compose (5.1)–(5.2) into a single second-order ODE,

$$\frac{\mathrm{d}^2 R_m}{\mathrm{d}\tau} + b_1 m^2 \left(b_1 - \frac{(b_1+1)^2}{b_1} \right) R_m = \mathrm{i} \left(\frac{\mathrm{d}f_m}{\mathrm{d}\tau} + b_1 m f^*_{-m} - m(b_1+1) f_m \right). \tag{5.3}$$

For $m = 1$, the forcing terms are $f_m = f^*_{-m} = 0$ so that (5.3) is homogeneous and we have the solution

$$\left.\begin{aligned} R_1(\tau) &= C_+ \mathrm{e}^{\sqrt{1+2b_1}\tau} + C_- \mathrm{e}^{-\sqrt{1+2b_1}\tau}, \\ R^*_{-1}(\tau) &= C_+ M_+ \mathrm{e}^{\sqrt{1+2b_1}\tau} + C_- M_- \mathrm{e}^{-\sqrt{1+2b_1}\tau}, \end{aligned}\right\} \tag{5.4}$$

where

$$M_+ = -\frac{(1+b_1+\sqrt{1+2b_1})}{b_1}, \quad M_- = -\frac{(1+b_1-\sqrt{1+2b_1})}{b_1}, \tag{5.5a,b}$$

and the complex constants $C_\pm$ are determined from the IC constant σ,

$$C_\pm = \pm \frac{\mathrm{i}(1+b_1-\sigma^* b_1 \mp \sqrt{1+2b_1})}{4\sqrt{1+2b_1}}. \tag{5.6}$$

Since $1 + 2b_1 = -1/p(\gamma)$, and $p(\gamma) > 0$ for $\gamma > 1$ (as for ideal gases) for any reasonable choice of γ (see § 6), the exponentials in (5.4) are purely oscillatory. Note also that $M_\pm$ are complex numbers with unity magnitude, so their effect in the $-m$ solution is that of a time-phase shift to each term.

The forcing term of (5.3) for $m = 2$ is

$$\begin{aligned} F_2 &= \frac{\mathrm{d}f_2}{\mathrm{d}\tau} + 2b_1 f^*_{-2} - 2(b_1+1) f_2 && (5.7) \\ &= 2(K_+ C_+^2 \mathrm{e}^{2\sqrt{1+2b_1}\tau} + K_- C_-^2 \mathrm{e}^{-2\sqrt{1+2b_1}\tau}) + O(1), && (5.8) \end{aligned}$$

where

$$\begin{aligned} K_+ &= (1-M_+^2) b_1^2 + (2M_+ + 1) b_1 (1 - \sqrt{1+2b_1}) && (5.9) \\ &\quad + (M_+ + 1)^2 (1 - \sqrt{1+2b_1}) b_2, && (5.10) \\ K_- &= (1-M_-^2) b_1^2 + (2M_- + 1) b_1 (1 + \sqrt{1+2b_1}) && (5.11) \\ &\quad + (M_- + 1)^2 (1 + \sqrt{1+2b_1}) b_2, && (5.12) \end{aligned}$$

and in fact $K_- = K_+^*$, and we have the corresponding particular solution

$$\left.\begin{aligned} R_2(\tau) &= \frac{\mathrm{i}\tau}{2\sqrt{1+2b_1}} (C_+^2 K_+ \mathrm{e}^{2\sqrt{1+2b_1}\tau} - C_-^2 K_- \mathrm{e}^{-2\sqrt{1+2b_1}\tau}) + O(1), \\ R^*_{-2}(\tau) &= \frac{\mathrm{i}\tau}{2\sqrt{1+2b_1}} (C_+^2 K_+ M_+ \mathrm{e}^{2\sqrt{1+2b_1}\tau} - C_-^2 K_- M_- \mathrm{e}^{-2\sqrt{1+2b_1}\tau}) + O(1), \end{aligned}\right\} \tag{5.13}$$

https://doi.org/10.1017/jfm.2018.263 Published online by Cambridge University Press

where the homogeneous part of the solution is held in the $O(1)$ term since it is dominated by the $O(\tau)$ particular integral. We note in passing this implies that the initial conditions to the $m=2$ mode do not contribute to its growth in the leading order, subject to the constraints specified in § 4. Comparison of (5.4) with (5.13) suggests the following ansatz for R_m,

$$R_m(\tau) = \tau^{m-1}\left[C_+^m\lambda_m^+ \mathrm{e}^{m\sqrt{1+2b_1}\tau} + C_-^m\lambda_m^- \mathrm{e}^{-m\sqrt{1+2b_1}\tau}\right] + O(\tau^{m-2}), \tag{5.14}$$

$$R^*_{-m}(\tau) = \tau^{m-1}\left[C_+^m M_+\lambda_m^+ \mathrm{e}^{m\sqrt{1+2b_1}\tau} + C_-^m M_-\lambda_m^- \mathrm{e}^{-m\sqrt{1+2b_1}\tau}\right] + O(\tau^{m-2}), \tag{5.15}$$

so that if the behaviour of λ_m for large m can be determined, then the leading-order asymptotic behaviour of the coefficients will be established.

5.2. *Recursion relation for coefficients*

The forcing terms are

$$\begin{aligned} f_m(\tau) &= -\sum_{r_1+r_2=m} r_1 r_2\,(b_1[R_{r_1}R^*_{-r_2} + R_{r_1}\{R_{r_2}+R^*_{-r_2}\}] \\ &\quad + b_2[R_{r_1}+R^*_{-r_1}][R_{r_2}+R^*_{-r_2}]) + \cdots, \end{aligned} \tag{5.16}$$

$$\begin{aligned} f^*_{-m}(\tau) &= -\sum_{r_1+r_2=m} r_1 r_2\,(b_1[R^*_{-r_1}R_{r_2} + R^*_{-r_1}\{R_{r_2}+R^*_{-r_2}\}] \\ &\quad + b_2[R_{r_1}+R^*_{-r_1}][R_{r_2}+R^*_{-r_2}]) + \cdots, \end{aligned} \tag{5.17}$$

$$F_m(\tau) = \frac{\mathrm{d}f_m}{\mathrm{d}\tau} + mb_1 f^*_{-m} - m(b_1+1)f_m, \tag{5.18}$$

which can be written more compactly as

$$F_m = \sum_{s=2}^{m}\left[\tau^{s-2}\sum_{q=0}^{m/2}\{\Gamma_s^{(q,+)}\mathrm{e}^{(m-2q)\sqrt{1+2b_1}\tau} + \Gamma_s^{(q,-)}\mathrm{e}^{-(m-2q)\sqrt{1+2b_1}\tau}\}\right]. \tag{5.19}$$

The upper bound on the second sum of (5.19) is taken as $(m-1)/2$ if m is odd. The coefficients $\Gamma_s^{(q,\pm)}$ (the superscripts and subscripts signify labels) can be determined explicitly from the lower mode solutions. It can be shown, first, that only the leading-order term $s=m$ contributes to the leading-order term of the solution R_m, and second, that within this term the only leading-order contributor is the $q=0$ subterm. The $s=m$ term corresponds to the second-order convolutions in the forcing term, thus justifying our earlier truncation to those terms. Now after identifying the constants $\Gamma_m^{(0,\pm)}$ by comparison with (5.18) and substituting in the form of the ansatz, after some algebra we obtain

$$\Gamma_m^{(0,+)} = mC_+^m K_+ \sum_{r_1+r_2=m} r_1 r_2 \lambda_{r_1}^+\lambda_{r_2}^+, \tag{5.20}$$

$$\Gamma_m^{(0,-)} = mC_-^m K_- \sum_{r_1+r_2=m} r_1 r_2 \lambda_{r_2}^-\lambda_{r_2}^-, \tag{5.21}$$

https://doi.org/10.1017/jfm.2018.263 Published online by Cambridge University Press

and using variation of parameters to solve for R_m gives

$$\left.\begin{aligned}\lambda_m^+ &= \frac{\mathrm{i}K_+}{2(m-1)\sqrt{1+2b_1}}\sum_{r_1+r_2=m} r_1 r_2 \lambda_{r_1}^+ \lambda_{r_2}^+,\\ \lambda_m^- &= \frac{(\mathrm{i}K_+)^*}{2(m-1)\sqrt{1+2b_1}}\sum_{r_1+r_2=m} r_1 r_2 \lambda_{r_1}^- \lambda_{r_2}^-.\end{aligned}\right\} \tag{5.22}$$

This proves the ansatz by induction since it holds for the cases $m=1,2$ with $\lambda_1^\pm = 1$, and (5.22) shows that if the $(m-1)$th solution follows the ansatz then the mth must as well.

5.3. *Asymptotic behaviour*

Equation (5.22) is a recursion relation for the $\lambda_m^\pm$ but still not enough to determine analytically their asymptotic behaviour. For this we utilize the generating-function method of Moore (1979) for the amplitudes,

$$g(x) = \sum_{m=1}^{\infty} |\lambda_m| x^m, \tag{5.23}$$

over x complex. The $\pm$-superscript is omitted since (5.22) implies $|\lambda_m^+| = |\lambda_m^-|$. Likewise, $|K_+| = |K_-|$. Given (5.22), (5.23) satisfies the ODE

$$\frac{\mathrm{d}}{\mathrm{d}x}\left(\frac{g(x)}{x}\right) = \frac{K_B}{2}\left(\frac{\mathrm{d}g}{\mathrm{d}x}\right)^2, \tag{5.24}$$

where $K_B = \mathrm{i}|K_\pm|/\sqrt{1+2b_1}$. Note that this ODE is similar in form to equation (3.8) of Moore (1979). This is because in both studies the quadratic in the system of inhomogeneous equations dominates the forcing term, leading to a recursion relation with the form of (5.22). Since $|\lambda_1| = 1$ there is the initial condition

$$g'(0) = 1, \tag{5.25}$$

giving the following solution to (5.24),

$$g(x) = -\frac{2W(-xK_B) + W^2(-xK_B)}{2K_B}, \tag{5.26}$$

where $W(x)$ is the principal branch of the Lambert W-function. Now $g(x)$ has a singularity in its derivative at $x_c = -(K_B e)^{-1}$, but is analytic everywhere else on the circle in complex x of radius $|x_c|$. Recall that we seek the behaviour of $|\lambda_m|$ as $m \to \infty$. For this we use Darboux's method (Olver 1974). We seek a comparison function $f(x)$ which is analytic in some disc around x_c, for which $g(x) - f(x)$ is continuous in that disc, and whose Laurent series expansion coefficients have known asymptotic behaviour. Then, the coefficients of the $g(x)$ generating function behave asymptotically like those of the $f(x)$ Laurent series. This comparison function is constructed as follows: $g(x)$ has a Laurent series expansion around x_c,

$$g(x) \simeq \frac{1}{2K_B} - \frac{1 - xK_B e}{K_B} + \frac{2\sqrt{2}(1 - xK_B e)^{3/2}}{3K_B} + \cdots. \tag{5.27}$$

https://doi.org/10.1017/jfm.2018.263 Published online by Cambridge University Press

The third term dominates singular behaviour in the derivative, and we identify it as $f(x)$, satisfying the requirements and having an expansion

$$f(x) = \frac{2\sqrt{2}(1 - exK_B)^{3/2}}{3K_B} = \sum_{m=0}^{\infty} a_m x^m, \tag{5.28}$$

with Darboux's method concluding via the binomial theorem asymptotically,

$$|\lambda_m| \sim a_m \simeq \frac{1}{\sqrt{2\pi}} K_B^{m+1} \mathrm{e}^m m^{-5/2}. \tag{5.29}$$

Hence we have the asymptotic form of the shock perturbation Fourier coefficients to leading order:

$$\begin{aligned} R_m(\tau) &= \mathrm{i}\tau^{m-1} K_B^{m+1} \mathrm{e}^m m^{-5/2} \\ &\quad \times (|C_+^m| \mathrm{e}^{m\sqrt{1+2b_1}\tau + \mathrm{i}Q_+} + |C_-^m| \mathrm{e}^{-m\sqrt{1+2b_1}\tau + \mathrm{i}Q_-}) + O(\tau^{m-1}), \qquad (5.30) \\ R_{-m}^*(\tau) &= \mathrm{i}\tau^{m-1} K_B^{m+1} \mathrm{e}^m m^{-5/2} \\ &\quad \times (|C_+^m| M_+ \mathrm{e}^{m\sqrt{1+2b_1}\tau + \mathrm{i}Q_+} + |C_-^m| M_- \mathrm{e}^{-m\sqrt{1+2b_1}\tau + \mathrm{i}Q_-}) + O(\tau^{m-1}), \qquad (5.31) \end{aligned}$$

where $Q_\pm = \arg(\lambda_m^\pm C_\pm^m)$. The generating function does not yield $\arg \lambda_m^\pm$ but this is not important since its only effect is a time-phase shift to the oscillating part of R_m. By definition of R_m, we then have

$$\begin{aligned} \hat{z}_m(\tau) &= \frac{\mathrm{i}K_B m^{-5/2}}{\tau} \exp(m(1 + \log[\tau K_B |C_+| \epsilon])) \{\mathrm{e}^{m\sqrt{1+2b_1}\tau + \mathrm{i}Q_+}\} \\ &\quad + \frac{\mathrm{i}K_B m^{-5/2}}{\tau} \exp(m(1 + \log[\tau K_B |C_-| \epsilon])) \{\mathrm{e}^{-m\sqrt{1+2b_1}\tau + \mathrm{i}Q_-}\} \\ &\quad + O(\epsilon^m \tau^{m-1}) + O(\epsilon^{m+1} \phi(\tau)), \end{aligned} \tag{5.32}$$

for $m > 0$, and similarly for z_{-m} recalling that $|M_+| = |M_-| = 1$. We remark that the above analysis does not explicitly consider the $m = 0$ mode. The highest-order contribution to the $m = 0$ mode comes from second-order convolution of the $|m| = 1$ terms, and so is an oscillatory function with $O(\epsilon^2)$. However it has no effect on any coefficients $m \neq 0$ because of the form of the forcing function.

5.4. *Time to singularity formation*

Our approach contains the combination of truncation with asymptotic analysis of the truncated system. We cannot justify this formally. Indeed, the order term involving $\phi(\tau)$ in (5.32) comes from the higher-order subsystems for $R_{m,j}$, $j \neq 0$, which have been neglected in this analysis. Therefore, in writing (5.32) we assume without proof that the unknown time dependence $\phi(\tau)$ is not so large that the first term ceases to be leading order. As noted by Moore (1979) for vortex-sheet evolution, 'the possibility that the expansion is not uniformly valid as m goes to infinity cannot be ruled out ... the conclusions drawn here must remain merely plausible'. But such a non-uniformity would imply that $\hat{z}_m$ is greater than $O(\epsilon^m)$ which is implausible in light of the reasoning in § 4. Thus, although we do not prove that the assumptions made in § 4 are correct, they are consistent with the neglect of $\phi(\tau)$. In § 9 we will discuss the numerical evidence further supporting this assumption. There are

https://doi.org/10.1017/jfm.2018.263 Published online by Cambridge University Press

two leading-order terms in (5.32). In each, the quantity in curled brackets is purely oscillatory, and the amplitude is controlled by the real exponent and the factor $m^{-5/2}$. Therefore, the shock profile remains analytic for as long as

$$1 + \log\left[\tau K_B C \epsilon\right] < 0, \tag{5.33}$$

where $C = \max\left(|C_+|, |C_-|\right)$, implying that a singularity forms in the geometry of the shock at the critical time,

$$\tau_c = \frac{\mathrm{e}^{-1}}{K_B C \epsilon}, \tag{5.34}$$

corresponding to whichever of the two leading terms in (5.32) first loses exponential decay. Using the definition of τ and K_B,

$$t_c = \frac{\mathrm{e}^{-1}|\sqrt{1+2b_1}|}{M_0 a_0 |K_\pm| C \epsilon}. \tag{5.35}$$

The constants K_+, K_- are given by (5.10), (5.11), themselves depending on $M_\pm$ given by (5.5) and b_1, b_2 given by (3.3) by setting $k = 1, 2$. These constants depend on Whitham's exponent $p(\gamma)$ calculated by (2.11), and for comparisons made here we use a specific heat ratio $\gamma = 5/3$. The constants C_+, C_- used in determining C are given by (5.6) and contain the effect of the IC through the choice of σ. Note that $C = |C_+|$ for $\mathrm{Im}(\sigma) \geqslant 0$ and $C = |C_-|$ for $\mathrm{Im}(\sigma) \leqslant 0$, and hence for real σ, $C = |C_+| = |C_-|$.

This completes the analysis for strong shocks. At time t_c, the Fourier coefficients cease to decay exponentially with mode number and hence analyticity is lost, or equivalently a singularity has formed in the shock geometry. Equation (5.35) suggests, firstly, that the formation time of the singularity occurs inversely proportional to amplitude. As implied by § 6 the form of this dependence is not restricted to the strong-shock limit, but the constant of proportionality in (5.34) is for this limit only. Singularity formation in a time that goes as ϵ^{-1} is in agreement with the numerical results and theoretical sketch provided in Mostert *et al.* (2017) for the gas-dynamic shock. We note in passing that this dependence is quite distinct from the result of Moore (1979) which predicts $t_c \propto \log \epsilon$ (with ϵ defined as in the present case). This difference arises because Moore's form for the Fourier coefficients involves a factor e^{mt} associated with perturbation amplitude growth for the vortex sheet, rather than the oscillatory behaviour of the propagating shock seen presently.

For the strong-shock limit, the constant is inversely proportional to the unperturbed shock speed $a_0 M_0$, directly proportional to the shock oscillation fundamental frequency $\omega_0 = \mathrm{Im}(\sqrt{1+2b_1})$ and in general is a function of γ and the initial condition via the constants $K_\pm$ and $C_\pm$. The dependency on γ ultimately comes in through b_1, b_2, which, in the strong-shock limit, depend on Whitham's exponent $p(\gamma)$. Some features of these dependencies are discussed in figure 1, in § 6.1.

The algebraic decay rate of $m^{-5/2}$ in (5.32) indicates a loss of analyticity in the shock shape. At this stage the nature of the implied singularity at $t = t_c$ is not apparent. We might identify this with the formation of a shock–shock, if it were a discontinuity in slope, but this is not consistent with an $m^{-5/2}$ decay in Fourier coefficients. This is considered further in § 8.2, where the character of the singularity is discussed, and also in § 9. Lastly, equation (5.32) (and the leading-order solution to the first Fourier mode) asserts that the shock perturbations oscillate with a fundamental frequency $\mathrm{Im}(\sqrt{1+2b_1})$ in time. The higher Fourier mode coefficients oscillate at a harmonic of this frequency, superimposed on polynomial growth in time.

https://doi.org/10.1017/jfm.2018.263 Published online by Cambridge University Press

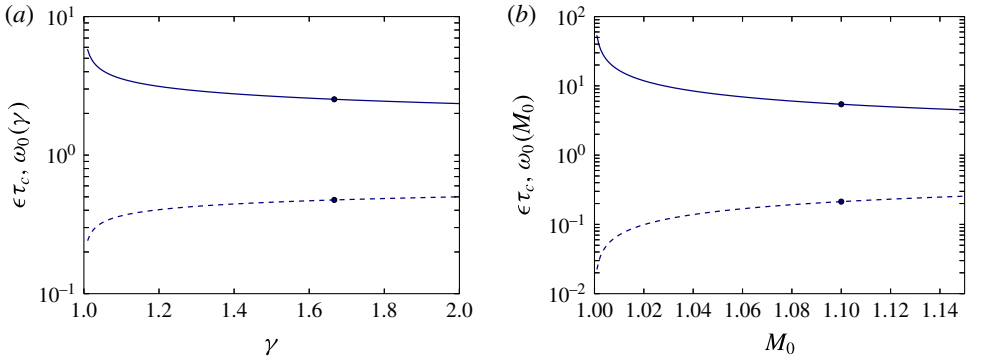


FIGURE 1. (Colour online) Variation of the proportionality constant for singularity formation, $\epsilon\tau_c$ and fundamental oscillation frequency $\omega_0 = \mathrm{Im}(\sqrt{1+2b_1})$ (with or without the overtilde on b_1) for (*a*) the strong-shock result of § 5 and (*b*) the weak-shock result § 6.1. In both parts, the dot shows the representative value of the parameter chosen in § 8. In (*a*), the constants depend only on γ, and in (*b*) only on unperturbed Mach number M_0. Note the similar limiting behaviour in either case in the limit $\gamma, M_0 \to 1$.

6. Weak-shock limit and general Mach number

We extend the prior results first to the small Mach-number limit, followed by the general M case. Although (2.15) and (2.9) are more complicated than (2.13), they are relatively simple to investigate if they can be written in a form similar to (3.1).

6.1. *Small Mach-number limit*

On defining

$$P(\beta,\sigma) = \sum_{k=1}^{\infty} c_k(\sigma)(Dz + Dz^* + DzDz^*)^k, \quad c_k(\sigma) = \binom{\sigma}{k}, \tag{6.1}$$

equation (2.15) becomes

$$\mathrm{i}a_0 M_0 + \frac{\partial z}{\partial t} = \mathrm{i}a_0 \left[(M_0 - 1)\left\{1 + P\left(\beta, -\frac{1}{4}\right)\right\} + 1\right](1 + Dz)\left\{1 + P\left(\beta, -\frac{1}{2}\right)\right\}. \tag{6.2}$$

Retaining up to quadratic terms as in the previous analysis, this may be written (suppressing β dependence for brevity)

$$\begin{aligned}\frac{\partial z}{\partial t} \simeq\ & \mathrm{i}a_0 \left[M_0\left\{P_2\left(-\frac{1}{4}\right) + P_2\left(-\frac{1}{2}\right) + Dz\right\} - P_2\left(-\frac{1}{4}\right)\right. \\ & + (M_0 - 1)\left\{\left[P_1\left(-\frac{1}{4}\right) + P_1\left(-\frac{1}{2}\right)\right]Dz + P_1\left(-\frac{1}{2}\right)P_1\left(-\frac{1}{4}\right)\right\} \\ & \left. + P_1\left(-\frac{1}{2}\right)Dz\right],\end{aligned} \tag{6.3}$$

https://doi.org/10.1017/jfm.2018.263 Published online by Cambridge University Press

where the $P_k(\sigma)$ denote partial sums of k terms. Define

$$\begin{aligned} Q(\beta,\sigma_1,\sigma_2) &= P(\beta,\sigma_1)+P(\beta,\sigma_2) \\ &= \sum_{k=1}^{\infty}(c_k(\sigma_1)+c_k(\sigma_2))(Dz+Dz^*+DzDz^*)^k \qquad (6.4) \\ N_1(\beta,\sigma_1,\sigma_2) &= P_1(\beta,\sigma_1)P_1(\beta,\sigma_2) \\ &= c_1(\sigma_1)c_1(\sigma_2)(Dz+Dz^*+DzDz^*)^2, \qquad (6.5) \end{aligned}$$

so that, again suppressing β dependence,

$$\frac{\partial z}{\partial t} \simeq ia_0\,[\,M_0\{Q_2(-1/4,-1/2)+Dz\}-P_2(-1/4) \qquad (6.6)$$

$$+(M_0-1)\{Q_1(-1/4,-1/2)Dz+N_1(-1/4)\}+P_1(-1/2)Dz\,]\,. \qquad (6.7)$$

Separating the first- and second-order terms, and defining, as for the strong-shock case, $\tau = a_0 M_0 t$,

$$\frac{1}{\mathrm{i}}\frac{\partial z}{\partial \tau} \simeq Dz+\tilde{b}_1(Dz+Dz^*)+\tilde{b}_1[DzDz^*+Dz(Dz+Dz^*)]+\tilde{b}_2(Dz+Dz^*)^2, \qquad (6.8)$$

where

$$\tilde{b}_1 = c_1\left(-\frac{1}{4}\right)\left[1-\frac{1}{M_0}\right]+c_1\left(-\frac{1}{2}\right), \qquad (6.9)$$

$$\tilde{b}_2 = \frac{M_0-1}{M_0}\left[c_1\left(-\frac{1}{4}\right)c_1\left(-\frac{1}{2}\right)\right]+c_2\left(-\frac{1}{4}\right)+c_2\left(-\frac{1}{2}\right)-\frac{1}{M_0}c_2\left(-\frac{1}{4}\right). \qquad (6.10)$$

After substituting the Fourier representations into (6.8) the analysis is analogous to the strong-shock case. Then (5.34) and (5.35) are reproduced except that b_1, b_2 are replaced in the calculation of all constants by $\tilde{b}_1, \tilde{b}_2$, given by (6.9) and (6.10). One key difference is that for the weak-shock case, the constants $\tilde{b}_1, \tilde{b}_2$ are functions only of M_0, and hence the singularity formation time t_c is a function of γ only through the sound speed a_0. Also, while in §§ 3–5, b_2 is a binomial coefficient of b_1, the same is not true for $\tilde{b}_1$ and $\tilde{b}_2$. This does not affect the analysis.

Figure 1 shows the behaviour of the proportionality constant for singularity formation $\epsilon\tau_c$ and the fundamental oscillation frequency ω_0 with respect to the relevant parameter for the strong- (γ) and weak-shock (M_0) cases. For the strong shock, as $\gamma \to 1$, then by (2.11) the parameter $p(\gamma)$ grows without bound, giving $b_1 \to -1/2$, $b_2 \to 3/8$, and in turn $\omega_0 \to 0$ along with $\epsilon\tau_c \to \infty$. In fact, the same limits are reached for $\tilde{b}_1, \tilde{b}_2$ as $M_0 \to 1$, and so the graphs appear similar respective to their parameters.

6.2. *General M*

The difficulty in the general M case is in obtaining an explicit $q(A) = f^{-1}(M)$. For both the strong- and weak-shock analysis it was found sufficient to truncate at quadratic convolution terms. This suggests treatment of the general M case under a second-order Taylor expansion of $f(M)$ around any M_0. The goal is to obtain a form like (6.8) in which the equivalent general coefficients, $\bar{b}_1, \bar{b}_2$, tend to the respective limiting cases $\tilde{b}_1, \tilde{b}_2$ as $M_0 \to 1$ and b_1, b_2 as $M_0 \to \infty$. The algebra is cumbersome, and so we

https://doi.org/10.1017/jfm.2018.263 Published online by Cambridge University Press

provide a sketch of the main result. The Taylor expansion of $f(M)$ can be written, rearranging the constants appropriately,

$$f(M) = \alpha_0(M_0, \gamma) + \alpha_1(M_0, \gamma)M + \alpha_2(M_0, \gamma)M^2 + O((M - M_0)^3), \tag{6.11}$$

where the coefficients $\alpha_i(M_0, \gamma)$, $i = 1, 2, 3$ can be determined numerically. Truncating to second order and solving the quadratic then gives the required $M = q(A)$. The analogue of (6.8) is then

$$\frac{1}{\mathrm{i}}\frac{\partial z}{\partial \tau} \simeq Dz + \bar{b}_1(Dz + Dz^*) + \bar{b}_1[DzDz^* + Dz(Dz + Dz^*)] + \bar{b}_2(Dz + Dz^*)^2, \tag{6.12}$$

where

$$\bar{b}_1 = c_1(-1/2) - \frac{\mathcal{A}\mathcal{B}}{M_0}c_1^2(1/2), \tag{6.13}$$

$$\bar{b}_2 = c_2(-1/2) - \frac{\mathcal{A}\mathcal{B}}{M_0}(c_1(1/2)c_2(1/2) + \mathcal{A}c_2(1/2)c_1^2(1/2) - c_1^3(1/2)), \tag{6.14}$$

$$\mathcal{A} = \frac{\mathcal{C}}{\mathcal{C} + \mathcal{D}}, \quad \mathcal{B} = \sqrt{\mathcal{C} + \mathcal{D}}, \tag{6.15a,b}$$

$$\mathcal{C} = \frac{\alpha_0 + \alpha_1 M_0 + \alpha_2 M_0^2}{\alpha_2}, \quad \mathcal{D} = \frac{\alpha_1^2 - 4\alpha_2\alpha_0}{4\alpha_2^2}. \tag{6.16a,b}$$

The analysis then proceeds as in the strong-shock case. The constants $\bar{b}_1, \bar{b}_2$ tend to the appropriate limiting cases as desired, and are functions of both γ and M_0.

7. Strong parallel MHD shocks

We now discuss fast mode MHD shocks for which the magnetic field is parallel to the mean shock position, and for which the magnetosonic Mach number $M_f = Ma_0/c_{f0} \gg 1$, where c_{f0} is the parallel magnetosonic speed in the upstream flow. In appendix A the area–Mach-number relation for MHD shocks is considered, with the result that the sonic M can be related to A by

$$\frac{M}{M_0} = \left(\frac{A}{A_0}\right)^{-1/p(\gamma)}(1 + O(\epsilon^2/M)), \tag{7.1}$$

where $p(\gamma)$ is given by (2.11). But in § 5.2 it is shown that only terms quadratic in ϵ need be retained, and in the large M_f and hence large M limit, the $O(\epsilon^2/M)$ correction on the right-hand side is sufficiently small to be neglected. Hence we recover (2.10), and the analysis of §§ 3–5 follows just as in the gas-dynamic strong-shock case, and (5.35) is reproduced identically for the time to formation of a singularity in the shock profile.

The above requires $M \gg 1$ in order to neglect the correction. Conversely, the condition $M \gg 1$ alone is insufficient for $M_f \gg 1$ in the case where the magnetic field is very strong relative to the pressure ahead of the shock. Indeed appendix A does not apply to MHD 'weak-shock' cases where $M_f - 1 \ll 1$ even if simultaneously $M \gg 1$. We do not consider such cases presently.

https://doi.org/10.1017/jfm.2018.263 Published online by Cambridge University Press

8. Comparison with numerical GSD

For the purposes of comparison of the analytical results with numerical solution of the full GSD equations we use the shock-dynamics code developed in Mostert *et al.* (2017) for magnetohydrodynamic fast shocks but here applied only to gas-dynamic shocks (that is, the field is defined to be zero). The code solves directly for the shock contour $\alpha(\xi, \eta)$ where (ξ, η) are general curvilinear coordinates with corresponding scale factors (S, T). The code advances the contour value in space by differentiating pseudospectrally in η and advancing with a Crank–Nicolson scheme in ξ. Here we run the code with $S = 1$, $T = 2\pi$ for comparison with the present analytic result.

The numerical method, which is of the type of Schwendeman (1993), is most conveniently initialized with a flat shock and some prescribed Mach-number perturbation. This can be specified by requiring that the initial perturbation $z(\beta, 0)$ be real, meaning that the ray-tube distribution on the shock, and hence the Mach-number distribution, is perturbed, but the shock shape is not. This is

$$z(\beta, 0) = \epsilon \sin(\beta), \tag{8.1}$$

$$\hat{z}_{\pm 1}(0) = \mp \mathrm{i}\frac{\epsilon}{2}, \tag{8.2}$$

hence $\sigma = z_{-1}/z_1 = -1$ (and hence $|C_+| = |C_-|$) corresponding to initial strong-shock A, M distributions of

$$A(\beta, 0) = A_0(1 + \epsilon \cos(\beta)), \quad M(\beta, 0) = M_0 A^{-1/p}, \tag{8.3a,b}$$

and weak-shock distributions

$$A(\beta, 0) = A_0(1 + \epsilon \cos(\beta)), \quad M(\beta, 0) = (A^{-1/2})(M_0 - 1) + 1. \tag{8.4a,b}$$

The perturbation ϵ is defined by (4.3) in § 4 while the corresponding amplitude of the Mach-number perturbation is $M_0\epsilon/p$. Without loss of generality we can choose $A_0 = L = 1$. We consider strong- and weak-shock cases $M_0 = 50, 1.1$ respectively with $\epsilon = 0.1, 0.08, 0.06, 0.04, 0.02, 0.01$. The function extending to higher Fourier modes is $h(1) = 1$, and $h(m) = 0$ for $m \neq 1$. The extent of η and ξ is identified with the real and imaginary parts of $Z(\beta, t)$ respectively. The numerical resolution for the cases run here is $N_\eta = 2048$ and $\mathrm{d}\xi = \epsilon/40$, although for $M_0 = 50$, $\epsilon = 0.1, 0.08$ the resolution is $\mathrm{d}\xi = \epsilon/80$.

8.1. *Time to shock–shock formation*

In the numerical GSD code, shock–shocks are detected with a spectral edge detector (Gelb & Tadmor 1999) which is applied on the Mach-number profile extracted from contours of the time-like parameter α. The detector uses a minmod-type limiter which chooses between a first-order concentration kernel close to discontinuities in the Mach number and an exponential kernel away from discontinuities (Gelb & Tadmor 2000), and an additional nonlinear enhancement technique (Gelb & Tadmor 2006). This technique relies on a parameter $\Delta M_r/N_\eta$ which is the smallest expected jump in Mach number on the shock associated with the formation of a shock–shock, scaling with the resolution in η. Although t_s is largely insensitive to the enhancement parameter, possible variations in its choice along with some methodological details suggest an estimated uncertainty of approximately 5 %–6 % in the final values. The Mach number along a given shock contour is obtained by a simple nearest-cell interpolation routine,

https://doi.org/10.1017/jfm.2018.263 Published online by Cambridge University Press

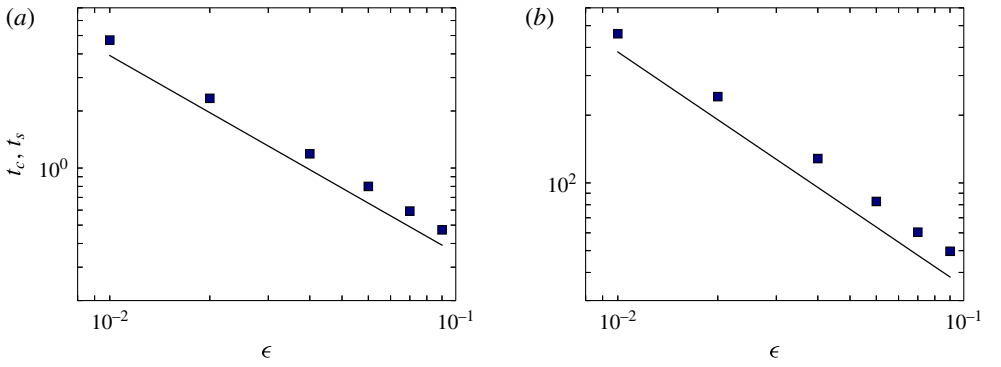


FIGURE 2. (Colour online) Comparison of analytical singularity times t_c, calculated from (5.35), and numerical shock–shock formation times t_s, collectively called critical times for (*a*) strong shocks, $M_0 = 50$ and (*b*) weak shocks, $M_0 = 1.1$. $\gamma = 5/3$ for these cases; ——, t_c; ■ (navy), t_s.

and the value of t_s is effectively grid-converged to within 2 % for resolution in both ξ and η directions for tested points, accounting for the parameter-dependent effects. We distinguish between the time to shock–shock formation t_s obtained in this way and the analytical result for time to singularity formation t_c, for reasons that will be discussed fully in § 9, but refer to both times as critical times for the sake of comparison.

Figure 2 shows the data for the analytical result compared with some points collected from the numerical method, with $\gamma = 5/3$. The analytical result underestimates the numerical t_s at the largest amplitudes by approximately 15 %–26 %. For both cases, the agreement between t_c and t_s tends to improve slightly as ϵ is decreased. These discrepancies are discussed further in § 9.

8.2. *Analytical shock shape construction*

Although the focus of § 5 is the asymptotic behaviour of the λ_m, and hence the $\hat{z}_m(\tau)$, at high m, the recursion relation (5.22) may be used in the form for $R_m(\tau)$, equation (5.15), and from there in (4.6). Provided the recursion relation is not catastrophically unstable, this generates the leading order of the Fourier coefficients up to some high m, say 512, and may then be used in the Fourier series to reconstruct the physical shock shape, which can in turn be compared with the numerical results from the GSD code. This comparison for $M_0 = 50$, $\epsilon = 0.08$ is shown in figure 3.

The shock profiles obtained from the reconstructed analytical result and the GSD numerical solutions are qualitatively quite similar. In fact a further comparison can be drawn in shock oscillation time. At early times, the shock profile should remain smooth and roughly sinusoidal. During this early stage the fundamental frequency of oscillation of the shock can be determined. The analytically predicted time for a single oscillation t_{osc} can be calculated from the fundamental frequency,

$$t_{osc} = \frac{2\pi}{M_0 a_0 \mathrm{Im}(\sqrt{1 + 2b_1})}, \tag{8.5}$$

which for the case of $M_0 = 50$ shown in figure 3 is $t_{osc} \simeq 0.205$. The result found using GSD numerics differs by approximately 2.4 % from the predicted result, and this close

https://doi.org/10.1017/jfm.2018.263 Published online by Cambridge University Press

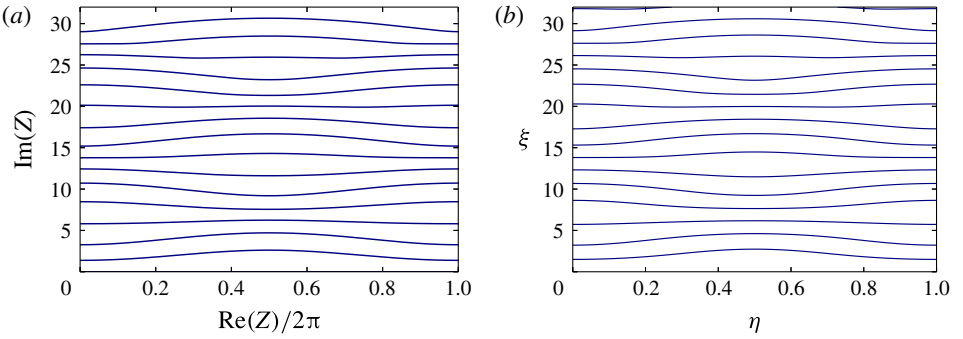


FIGURE 3. (Colour online) Comparison of analytical reconstruction of shock shape (*a*) with numerical GSD results (*b*) for $M_0 = 50$, $\epsilon = 0.08$. The GSD results are contours of the quantity $M_0\alpha$, which is equivalent to τ in the analytical results. Contours are plotted in increments of $\Delta\tau = \Delta(M_0\alpha) = 2$. The shock is travelling upwards and amplitudes are artificially amplified twentyfold for visibility. Im(Z) is equivalent to ξ and is the coordinate parallel to mean shock motion; Re(Z) is equivalent to η and is the coordinate perpendicular to mean shock motion. In (*a*), the uppermost contour just precedes the singularity formation predicted by (5.35), at $\tau_c = 31.614$.

agreement in shock oscillation time is visible qualitatively in figure 3. This oscillation time is not a function of perturbation amplitude.

A comparison may also be drawn between the Mach-number profiles during a given time bracket. Figure 4 compares the analytical reconstruction with the numerical result during a time window well before either critical time (figure 4*a*,*b*) and immediately before τ_c (figure 4*c*,*d*). The results are similar qualitatively in the former case, with opposite-travelling waves on the shock first colliding and then diverging along the shock. Physically, shock–shock formation corresponds to the steepening of these waves into discontinuities as $t \to t_s$; for the times just before τ_c, the analytically constructed profiles are steeper than the GSD result.

Some insight into the character of the singularity at $t = t_c$ can be obtained by examining the shock shape, slope and curvature as $\tau \to \tau_c$. Figure 5 shows the analytically reconstructed shock shape, slope (defined $\varsigma = \mathrm{Im}(Z')/\mathrm{Re}(Z')$) and curvature,

$$\kappa = \frac{\sqrt{(Z'.Z'^*)(Z''.Z''^*) - [(Z'.Z''^* + Z'^*.Z'')/2]^2}}{(Z'.Z'^*)^{3/2}}, \tag{8.6}$$

primes indicating differentiation with respect to β. The quantities Z', Z'' were obtained by summing term-by-term differentiation of the Fourier series of Z with 2048 Fourier coefficients. This is valid provided Z, Z' remain continuous. Derivatives of higher order than Z'' do not exist owing to the decay rate $m^{-5/2}$ of the Fourier coefficients.

As $\tau \to \tau_c$, figure 5(*a*) shows that the shock profile appears to be evolving toward the formation of two kinks, or slope discontinuities. In figure 5(*b*), the asymmetric (about $\mathrm{Re}(Z)/(2\,\pi) = 0.5$) slope is plotted in $0 \leqslant \mathrm{Re}(Z)/(2\,\pi) < 0.5$ while the symmetric curvature κ is plotted in $0.5 < \mathrm{Re}(Z)/(2\,\pi) < 1.0$. The slope is everywhere finite at $\tau = \tau_c$ but is approaching a discontinuity, while the curvature appears to exist everywhere except possibly at two isolated points where Z'' may become singular. It can be seen that the maximum shock curvature increases, as $\tau \to \tau_c$, along two converging, oblique lines in the Re(Z)–Im(Z) plane. This effect can also be observed as a prelude to shock–shock formation in figure 2(*a*) of Mostert *et al.* (2017).

https://doi.org/10.1017/jfm.2018.263 Published online by Cambridge University Press

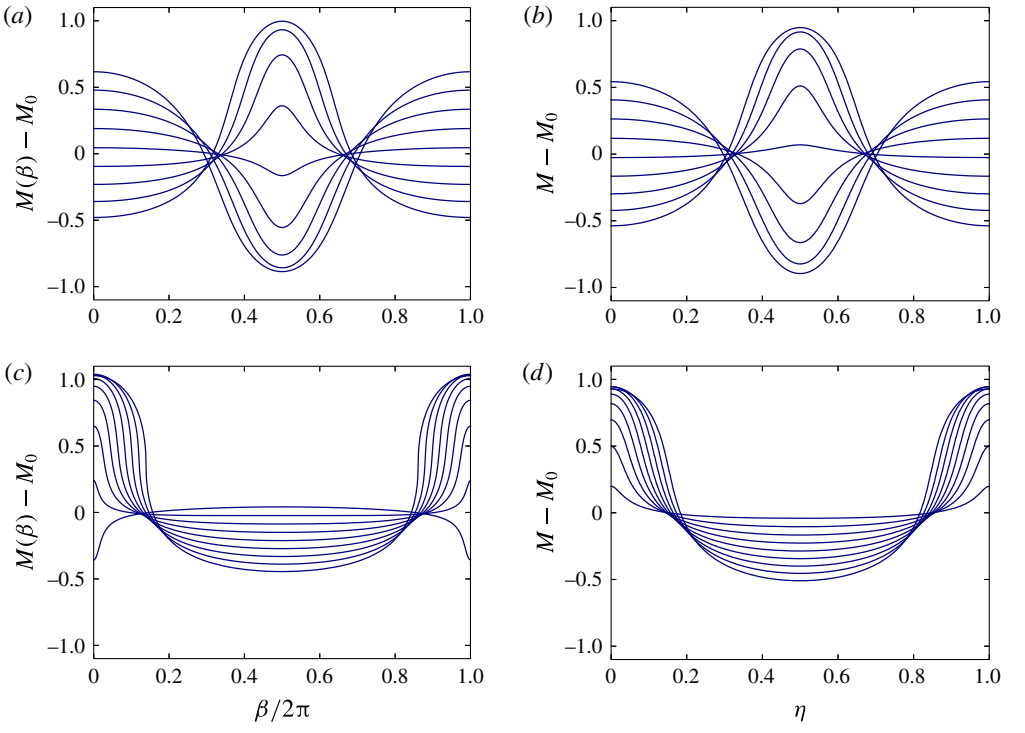


FIGURE 4. (Colour online) Mach-number profiles on the shock plotted (*a*,*b*) over time periods $\tau = [21, 25]$ with increments $\Delta\tau = \Delta(M_0\alpha) = 0.5$, and (*c*,*d*) $\tau = [29.614, 31.614]$ with increments $\Delta\tau = 0.25$. τ increasing on the left from top to bottom (*a*,*b*); from bottom to top (*c*,*d*). The last curve in (*c*,*d*) corresponds to $\tau_c = 31.614$. Analytical construction (*a*,*c*), calculated by central differences on the reconstructed shock profile; GSD numerical result (*b*,*d*), found by nearest-point interpolation on extracted contours of $M_0\alpha$. The case is $M_0 = 50$, $\epsilon = 0.08$. For the numerical result, $M_0 = \langle M \rangle$ along the profile.

8.3. *MHD strong-shock dependence on magnetic field strength*

Finally we examine the effect of varying magnetic field on t_s for perturbed parallel strong MHD shocks. The code of Mostert *et al.* (2017) is used with a non-zero magnetic field. The full area–Mach-number ODE is adjusted accordingly and the shock-detection routine remains unchanged. We test the same initial conditions as the gas-dynamic strong-shock case above, $M_0 = 50$, with a single representative perturbation amplitude $\epsilon = 0.05$, with uniform magnetic fields $B_0 = 0.2$, 0.5, 1, 10, 60. This corresponds to unperturbed fast magnetosonic Mach numbers of $M_{f0} = 49.4$, 46.6, 39.5, 6.4, 1.08. The condition that $M_f \gg 1$ is marginal in the case $B_0 = 10$, and clearly not met in the case $B_0 = 60$; these are included for comparison. For $B_0 = 60$ particularly it is not clear that (8.3) is the relevant initial condition for the numerical comparison since the analysis of appendix A does not apply.

Table 1 compares critical times for the strong-shock MHD case. As expected from the correspondence of the MHD *A*–*M* relation to the gas-dynamic case, critical times are insensitive to magnetic field strength for sufficiently small values. The relative differences are similar to those observed in the previous gas-dynamic comparisons. The strong-field case, in which $M_{f0} \simeq 1$, shows a different t_s as expected. Note that

https://doi.org/10.1017/jfm.2018.263 Published online by Cambridge University Press

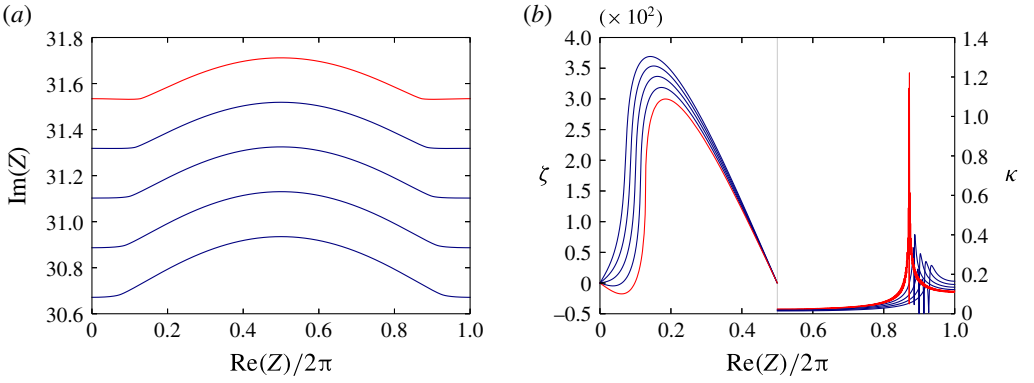


FIGURE 5. (Colour online) (*a*) Shock-profile perturbation amplified fourfold, (*b*) split plot of slope ς (left half) and curvature κ (right half). Profiles plotted $\tau \leqslant \tau_c$ up to $\tau_c = 31.6146$ at increments of $\Delta\tau = 0.2$, with the profile at τ_c in red. The line $\mathrm{Re}(Z)/2\pi = 0.5$ is a symmetry axis for κ and an antisymmetry axis for ς. $M_0 = 50$, $\epsilon = 0.08$, $\gamma = 5/3$ for this case.

$\lvert B_0\rvert$	M_{f0}	t_c	t_s	Δ_r
0.2	49.4	0.783	0.986	20.6 %
0.5	46.6	0.783	0.986	20.6 %
1.0	39.5	0.783	0.987	20.7 %
10	6.4	0.783	0.931	16.9 %
60	1.08	N/A	1.21	N/A

TABLE 1. Comparison of time to shock–shock formation for parallel MHD shocks. Δ_r is the relative difference of the analytical singularity formation time t_c to the numerically determined shock–shock formation time t_s. The strong-shock condition is not met in the case $B_0 = 60$ so the analytical result does not apply.

the case $B_0 = 10$, with a large but not truly strong M_{f0}, shows some difference to the other cases.

9. Discussion

Although a constraint is imposed on the function $h(m)$ in (4.5), this function does not appear in the subsequent analysis. This is because the IC appears in the leading-order term only for the solution to the first mode, $R_1(\tau)$, which in turn only depends on the first mode of the IC. For higher modes, the corresponding mode of the IC appears only in the homogeneous part of the solution, which does not contribute to leading order. Interestingly therefore, the nonlinear contribution from the first mode of the shock perturbation dominates all other contributions to any given mode independent of our choice of $h(m)$ so long as $h(m)$ grows at most algebraically with m. This emphasizes the strongly nonlinear nature of this problem. Thus our solution suggests that the time to singularity formation in a perturbed shock is, to leading order, independent of whether the perturbation is uni- or multimodal, provided that it is spatially periodic. We also remark that the stability of the shock, in the sense that the amplitude of a smooth perturbation on the shock surface will either grow or

https://doi.org/10.1017/jfm.2018.263 Published online by Cambridge University Press

decay over time, is not exposed explicitly by this analysis, unlike in other analyses such as that of Freeman (1957). This behaviour is probably a higher-order effect not captured by our method. A similar result and explanation is noted by Denet *et al.* (2015) in their analysis of shock perturbations resulting from shock–vortex interaction. By comparison, the numerical GSD results presented here do exhibit an amplitude decay as expected, and this may account for part of the discrepancy between our analytical and numerical results (see below).

As discussed in § 8, the numerical and analytical results show discrepancies of up to 26 %. This is possibly due to neglect of the higher-order terms. Another interpretation is that t_c, the time to singularity formation predicted by the present study, and t_s, the numerical determination of shock–shock formation time, do not strictly correspond to the same phenomenon. A shock–shock is a discontinuity in shock slope that corresponds to a decay rate of m^{-2}. But this is not the decay rate of $m^{-5/2}$ seen in the analysis. Plots of the shock slope and curvature at the critical time obtained from spectral differentiation of the shock shape indicate that, at the critical time, the shock slope is continuous everywhere while the shock curvature is finite everywhere but appears to diverge at two isolated points within one spatial period. Further, we note that in the analytical result shown in figure 4(*c*), the Mach-number profiles appear to be developing two points of large slope, and differentiation of (2.7) suggests that this corresponds to those points at which $Z''(\beta)$ fails to exist. This suggests that shock–shock formation at t_s is preceded by the first appearance of isolated singularities in the shock curvature and Mach-number slope on the shock at $t_c < t_s$. This distinction between this first singularity formation and shock–shock formation cannot be resolved by the present analysis since the latter is valid only for $t < t_c$. But it could serve as a partial explanation for the differences between our analytical and numerical GSD results.

Two other observations concerning the comparison between numerical and analytical results are that first, the analysis makes several approximations with similar limitations to that of Moore (1979) and assumes uniform validity in m as $m \to \infty$, as well in time τ. Hence we neglect $\phi(\tau)$ in (5.32). In addition to arguments made in § 5, observe that if this assumption were invalid, then (5.32) would overestimate t_c, not underestimate it as in figure 2. Second, the numerical results also capture the decay of the perturbation over time, which is not reflected in the analysis. This may have the effect of decreasing the effective ϵ as time progresses in the numerical result, delaying the formation of shock–shocks and providing an additional source of discrepancy.

The analysis presented here applies strictly to an initial disturbance that is periodic on the shock. We cannot rule out that a different disturbance type, for example an initial perturbation that is spatially compact with a continuous spectrum, would yield a different dependence of t_c on some measure of the perturbation amplitude than found presently. This is suggested by analogy with the Burgers equation; see for example Whitham (2011).

Quantitative comparison of the present results with those of Clavin (2013), Denet *et al.* (2015) and Lodato *et al.* (2016, 2017) is uncertain since their boundary conditions are generally not spatially periodic but are based on a shock–vortex interaction perturbation and so the initial conditions do not match between formulations.

10. Concluding remarks

Using a spectral treatment of the shock-dynamics equations, we have developed an analysis showing that a spatially periodic plane-propagating, gas-dynamic shock wave

https://doi.org/10.1017/jfm.2018.263 Published online by Cambridge University Press

subject to a smooth, small perturbation amplitude of nominal magnitude ϵ, loses analyticity in a finite time. The governing geometrical shock-dynamics equations are first written as a single complex-valued partial differential equation describing the shock profile parametrized by a ray-tube labelling parameter β. An asymptotic analysis of the leading order of the Fourier coefficients in β is developed. This shows that the time to loss of analyticity is $t_c \propto \epsilon^{-1}$ with a proportionality constant which is in general a function of the unperturbed Mach number M_0 and specific heat ratio γ. Owing to the complicated form of the algebraic decay in the Fourier coefficients at the critical time, the physical character of the predicted loss of analyticity is difficult to determine. Numerical reconstruction of shock slope and curvature profiles at the critical time suggests that loss of analyticity corresponds to the onset of isolated curvature and Mach-number slope singularities while the shock slope itself remains everywhere continuous.

In comparison with numerical solutions of the underlying equations of geometrical shock dynamics, the analysis underestimates t_c with respect to the shock–shock formation time t_s, particularly for larger values of ϵ. While some limitations to the present analysis have been discussed that may contribute to this discrepancy, it is recognized that t_c and t_s do not strictly correspond to the same physical phenomenon. A reasonable hypothesis is that, at least for the presently considered perturbed planar shock waves, loss of analyticity in the shock shape at $t = t_c$ generally precedes true shock–shock formation at the somewhat later time $t = t_s$. The restricted MHD case considered here shows that in the strong-shock limit, parallel MHD shocks behave similarly to gas-dynamic shocks. Finally, the present analysis is not limited to nominally planar shock geometries but can, in principle, be extended to other two-dimensional geometries such as cylindrical implosions.

Acknowledgement

This research was supported by the KAUST Office of Sponsored Research under award URF/1/2162-01.

Appendix A. Area–Mach-number relation for strong parallel MHD shocks

We derive the asymptotic area–Mach-number relation for perturbed magnetohydrodynamic (MHD) shocks for which the magnetic field is parallel to the shock in the mean, and for which the magnetosonic Mach number $M_f \gg 1$. We begin with the general (in two dimensions) A–M–$\phi - x$ relation of Mostert *et al.* (2017) simplified accordingly for uniform fields into an A–M–ϕ relation,

$$\boldsymbol{e}_L \cdot \left[\frac{\partial \boldsymbol{v}}{\partial \phi}\, d\phi + \frac{\partial \boldsymbol{v}}{\partial M}\, \mathrm{d}M + \frac{1}{u_n + c_f} \boldsymbol{s} \frac{\mathrm{d}A}{A} \right] = 0, \tag{A 1}$$

where $v = \boldsymbol{v} = \{\rho, u_n, u_t, p, B_n, B_t\}^{\mathrm{T}}$, and

$$\boldsymbol{s} = \left\{ \rho u_n,\ \frac{B_t^2 - \rho u_t^2}{\rho},\ \frac{\rho u_n u_t - B_n B_t}{\rho},\ \rho a^2 u_n,\ 0,\ 0 \right\}^{\mathrm{T}}, \tag{A 2}$$

$$\boldsymbol{e}_L = \left\{ 0,\ \frac{\rho c_f^2 - B_n^2}{c_f},\ -\frac{B_n B_t}{c_f},\ \left(1 - \frac{B_n^2}{\rho c_f^2}\right),\ -\frac{u_t B_t}{u_n + c_f},\ B_t \right\}^{\mathrm{T}}, \tag{A 3}$$

$$c_f^2 = \frac{1}{2\rho} \left(\gamma p + B^2 + \sqrt{(\gamma p + B^2)^2 - 4\gamma p B_x^2} \right). \tag{A 4}$$

The flow variables here are interpreted as post-shock conditions except for M, ϕ.

https://doi.org/10.1017/jfm.2018.263 Published online by Cambridge University Press

A.1. *Jump conditions*

The calculation of post-shock conditions hinges on values r, b (see Wheatley, Pullin & Samtaney (2005)) as follows. Firstly,

$$r = \frac{1}{6\mathcal{A}}(-2\mathcal{B} + J + H), \tag{A 5}$$

where

$$H = 2^{2/3}\left(-N + \sqrt{-4(\mathcal{B}^2 - 3\mathcal{A}\mathcal{C})^3 + N^2}\right)^{1/3}, \tag{A 6}$$

$$J = 4(\mathcal{B}^2 - 3\mathcal{A}\mathcal{C})/H, \quad N = 2\mathcal{B}^3 - 9\mathcal{A}\mathcal{B}\mathcal{C} + 27\mathcal{A}^2\mathcal{D}, \tag{A 7a,b}$$

$$\mathcal{A} = \frac{\gamma+1}{\gamma-1}, \quad \mathcal{B} = -1 - \frac{2}{(\gamma-1)M^2} - B_0^2\frac{2(\gamma+1)\cos^2\phi + \gamma\sin^2\phi}{(\gamma-1)\gamma M^2}, \tag{A 8a,b}$$

$$\mathcal{C} = B_0^4\frac{(\gamma+1) + (4 + M^2(3\gamma-4))\gamma/B_0^2 + ((\gamma+1) + (4+M^2\gamma)\gamma/B^2)\cos 2\phi}{2(\gamma-1)M^4\gamma^2}, \tag{A 9}$$

$$\mathcal{D} = -B_0^4\frac{\cos^2\phi(1 + (\gamma-1)M^2 + \cos(2\phi))}{(\gamma-1)M^6\gamma^2}. \tag{A 10}$$

Secondly,

$$b = \frac{Y}{X}\sin\phi, \tag{A 11}$$

where $X = r - B_0^2\cos^2\phi/(M^2\gamma)$, $Y = 1 - B_0^2\cos^2\phi/(M^2\gamma)$. Then the post-shock density $\rho = 1/r$, normal velocity, $u_n = a_0M(1-r)$, tangential magnetic field $B_t = B_0b$, normal field $B_n = B_0\cos\phi$ and the pressure and tangential velocity,

$$p = 1 + \gamma M^2\left(1 - r - B_0^2\frac{b^2 - \sin^2\phi}{2M^2\gamma}\right), \quad u_t = -\frac{B_0^2}{M}\frac{(b - \sin\phi)\cos(\phi)}{\gamma}. \tag{A 12a,b}$$

A.2. *Strong perturbed parallel shocks*

We consider shocks for which $M_f \gg 1$. Defining the Alfvén speed $c_{A0} = B_0$, fast magnetosonic speed in a parallel field $c_{f0} = \sqrt{a_0^2 + c_{A0}^2}$ the Alfvén Mach number M_A, and the shock speed U we have $M_f = Ma_0/c_{f0} = M_Ac_{A0}/c_{f0}$, so that $M_f \gg 1$ implies $M \gg 1$ and $M_A \gg 1$ (the converse is not true) so that $U \gg a_0$ and $U \gg c_{A0}$ in turn. Thus $M \gg c_{A0}/a_0$. Hence if $a_0 = O(1)$ then $M \gg B_0$ (recall physical variables are non-dimensional). Next, we make the substitution $\theta = \pi/2 - \phi$ and consider the jump conditions for small perturbations around the parallel field $\theta \ll 1$. This greatly simplifies the jump conditions,

$$r = \frac{1}{\rho} = \frac{\gamma-1}{\gamma+1} + O(1/M^2) + O(\theta^2/M^2), \tag{A 13}$$

$$b = \frac{\gamma+1}{\gamma-1}\left(1 - \frac{\theta^2}{2} + O(1/M^2) + O(\theta^2/M^2)\right), \tag{A 14}$$

$$u_n = \frac{2M\sqrt{\gamma}}{\gamma+1}(1 + O(1/M^2) + O(\theta^2/M^2)), \tag{A 15}$$

https://doi.org/10.1017/jfm.2018.263 Published online by Cambridge University Press

$$u_t = \frac{\theta B_0^2}{\gamma M}\left(\frac{2}{\gamma+1} + O(1/M^2) + O(\theta^2/M^2)\right), \tag{A 16}$$

$$p = \frac{2\gamma M^2}{\gamma+1}(1 + O(1/M^2) + O(\theta^2/M^2)), \quad B_n = B_0\theta + O(\theta^3), \tag{A 17a,b}$$

$$B_t = \frac{B_0(\gamma+1)}{\gamma-1}\left(1 - \frac{\theta^2}{2}\right)(1 + O(1/M^2) + O(\theta^2/M^2)), \tag{A 18}$$

$$c_f^2 = \frac{\gamma p + B^2}{\rho}(1 + O(\theta^2/M^2)) = \frac{\gamma p}{\rho}(1 + O(1/M^2) + O(\theta^2/M^2)), \tag{A 19}$$

where we retain separate order terms for θ where appropriate. Note that ρ, u_n, p, c_f are identical to the gas-dynamic case and independent of θ to leading order. The derivatives of these conditions with respect to M, θ are also required. By direct differentiation of the above, checked numerically, we obtain

$$\frac{\partial u_n}{\partial M} \sim \frac{2\sqrt{\gamma}}{\gamma+1}, \quad \frac{\partial B_n}{\partial M} = 0, \quad \frac{\partial p}{\partial M} \sim \frac{4\gamma M}{\gamma+1}, \tag{A 20a–c}$$

$$\frac{\partial B_t}{\partial M} = O(1/M^3), \quad \frac{\partial u_t}{\partial M} \sim -\frac{\theta B_0^2}{\gamma M^2}\left(\frac{2}{\gamma+1}\right), \tag{A 21a,b}$$

$$\frac{\partial u_n}{\partial \theta} = O(\theta/M), \quad \frac{\partial u_t}{\partial \theta} \sim \frac{B_0^2}{\gamma M}\left(\frac{2}{\gamma+1}\right), \quad \frac{\partial p}{\partial \theta} = O(\theta), \tag{A 22a–c}$$

$$\frac{\partial B_n}{\partial \theta} = B + O(\theta^2), \quad \frac{\partial B_t}{\partial \theta} = O(\theta). \tag{A 23a,b}$$

Equation (A 1) is

$$\psi_1\,\mathrm{d}\phi + \psi_2\,\mathrm{d}M + \psi_3\frac{\mathrm{d}A}{A} = 0, \tag{A 24}$$

where the functions $\psi_1 = \boldsymbol{e}_L \cdot \partial\boldsymbol{v}/\partial\phi$, $\psi_2 = \boldsymbol{e}_L \cdot \partial\boldsymbol{v}/\partial M$, $\psi_3 = \boldsymbol{e}_L \cdot \boldsymbol{s}/(u_n + c_f)$. These can be written in terms of their leading-order contributions,

$$\psi_1 \sim \frac{\partial p}{\partial\theta} + \frac{\partial B_t}{\partial\theta} = O(\theta), \quad \psi_2 \sim \frac{\partial p}{\partial M} + \rho c_f\frac{\partial u_n}{\partial M} = \frac{2\gamma M}{\gamma+1}\left[2 + \sqrt{\frac{2\gamma}{\gamma-1}}\right], \tag{A 25a,b}$$

$$\psi_3 \sim \frac{\rho a^2 u_n}{u_n + c_f} = \frac{4\gamma^2 M^2}{\gamma+1}\frac{1}{2 + \sqrt{2\gamma(\gamma-1)}}. \tag{A 26}$$

Dividing through by ψ_3, the second and third terms of (A 24) can be integrated,

$$-\int_0^\theta \frac{\psi_1}{\psi_3}\,\mathrm{d}\theta' + \Pi(\gamma)\log\frac{M}{M_0} + \log\frac{A}{A_0} = 0, \tag{A 27}$$

where $\Pi(\gamma)$ is given by (2.11) (noting $p(\gamma)$ in that equation is distinct from the post-shock pressure shown here), and primes denote integration variables. The bounds of

https://doi.org/10.1017/jfm.2018.263 Published online by Cambridge University Press

integration reflect integration from the unperturbed (lower) to the perturbed (upper) condition. We thus obtain

$$\frac{M}{M_0} \sim \left(\frac{A}{A_0}\right)^{-1/\Pi(\gamma)} \exp\left(\int_0^\theta \frac{\psi_1}{\psi_3}\,\mathrm{d}\theta'\right). \tag{A 28}$$

This result is equivalent to the gas-dynamic case if the exponential on the right-hand side is sufficiently close to unity to neglect. We have

$$\frac{\psi_1}{\psi_3} = \frac{q(\gamma)}{M^2} O(\theta), \tag{A 29}$$

$$\frac{|\psi_1||q(\gamma)|}{M^2} \leqslant \frac{\Psi|q(\gamma)|\theta}{M^2}, \tag{A 30}$$

$$\int_0^\theta \left|\frac{\psi_1}{\psi_3}\right| \mathrm{d}\theta' \leqslant \Psi q(\gamma) \int_0^\theta \frac{\theta'}{M^2}\,\mathrm{d}\theta', \tag{A 31}$$

with $q(\gamma)$ known and Ψ is some finite real positive constant. Using integration by parts, the integral on the right-hand side is

$$\int_0^\theta \frac{\theta'}{M^2}\,\mathrm{d}\theta' = \frac{\theta^2}{2M^2(\theta)} - \int_0^\theta \frac{\theta'^2}{M^3(\theta')}\frac{\partial M}{\partial \theta'}\,\mathrm{d}\theta'. \tag{A 32}$$

This is $O(\theta^2/M^2)$ assuming $\partial M/\partial\theta$ is small from the following observation. Equation (A 24) expresses the dependence of the differential change $\mathrm{d}M$ on $\mathrm{d}\theta$, $\mathrm{d}A$. But dividing through by ψ_2 shows that a change $\mathrm{d}\theta$ has at most $O(\theta/M)$ effect on $\mathrm{d}M$, hence the variation of M based on θ is small. Then the exponential on the right-hand side of (A 28) is $1 + O(\theta^2/M^2)$, acting as an MHD correction to the strong-shock gas-dynamic result. It can be shown that $\theta = O(\epsilon)$ so that

$$\frac{M}{M_0} \sim \left(\frac{A}{A_0}\right)^{-1/\Pi(\gamma)} (1 + O(\epsilon^2/M^2)), \tag{A 33}$$

for perturbed parallel MHD shocks for which $M_f \gg 1$.

REFERENCES

CHISNELL, R. F. 1957 The motion of a shock wave in a channel, with applications to cylindrical and spherical shock waves. *J. Fluid Mech.* **2**, 286–298.

CLAVIN, P. 2013 Nonlinear analysis of shock–vortex interaction: Mach stem formation. *J. Fluid Mech.* **721**, 324–339.

DENET, B., BIAMINO, L., LODATO, G., VERVISCH, L. & CLAVIN, P. 2015 Model equation for the dynamics of wrinkled shockwaves: comparison with DNS and experiments. *Combust. Sci. Technol.* **187** (1–2), 296–323.

FARIA, L. M., KASIMOV, A. R. & ROSALES, R. R. 2015 Theory of weakly nonlinear self-sustained detonations. *J. Fluid Mech.* **784**, 163–198.

FREEMAN, N. C. 1957 On the stability of plane shock waves. *J. Fluid Mech.* **2** (4), 397–411.

GELB, A. & TADMOR, E. 1999 Detection of edges in spectral data. *Appl. Comput. Harmon. Anal.* **7**, 101–135.

GELB, A. & TADMOR, E. 2000 Detection of edges in spectral data. Part II. Nonlinear enhancement. *SIAM J. Numer. Anal.* **38** (4), 1389–1408.

https://doi.org/10.1017/jfm.2018.263 Published online by Cambridge University Press

GELB, A. & TADMOR, E. 2006 Adaptive edge detectors for piecewise smooth data based on the *minmod* limiter. *J. Sci. Comput.* **28** (2/3), 279–306.

HENSHAW, W. D., SMYTH, N. F. & SCHWENDEMAN, D. W. 1986 Numerical shock propagation using geometrical shock dynamics. *J. Fluid Mech.* **171**, 519–545.

LODATO, G., VERVISCH, L. & CLAVIN, P. 2016 Direct numerical simulation of shock wavy-wall interaction: analysis of cellular shock structure and flow patterns. *J. Fluid Mech.* **789**, 221–258.

LODATO, G., VERVISCH, L. & CLAVIN, P. 2017 Numerical study of smoothly perturbed shocks in the Newtonian limit. *Flow Turbul. Combust.* **99**, 887–908.

MAJDA, A. & ROSALES, R. 1983 A theory for spontaneous Mach stem formation in reacting fronts. Part I. The basic perturbation analysis. *SIAM J. Appl. Maths* **43**, 1310–1334.

MOORE, D. W. 1979 The spontaneous appearance of a singularity in the shape of an evolving vortex sheet. *Proc. R. Soc. Lond.* A **365** (1720), 105–119.

MOSTERT, W., PULLIN, D. I., SAMTANEY, R. & WHEATLEY, V. 2017 Geometrical shock dynamics for magnetohydrodynamic fast shocks. *J. Fluid Mech.* **811**, R2.

OLVER, F. W. J. 1974 *Asymptotics and Special Functions*. Academic Press.

SCHWENDEMAN, D. W. 1993 A new numerical method for shock wave propagation based on geometrical shock dynamics. *Proc. R. Soc. Lond.* A **441** (1912), 331–341.

WATANABE, M. & TAKAYAMA, K. 1991 Stability of converging cylindrical shock waves. *Shock Waves* **1** (2), 149–160.

WHEATLEY, V., PULLIN, D. I. & SAMTANEY, R. 2005 Regular shock refraction at an oblique planar density interface in magnetohydrodynamics. *J. Fluid Mech.* **522**, 179–214.

WHITHAM, G. B. 2011 *Linear and Nonlinear Waves*. Wiley.

WHITHAM, G. B. 1957 A new approach to problems of shock dynamics. Part I. Two-dimensional problems. *J. Fluid Mech.* **2**, 145–171.

https://doi.org/10.1017/jfm.2018.263 Published online by Cambridge University Press